Applied Catalysis B: Environmental 218 (2017) 672–678

Contents lists available at ScienceDirect

Applied Catalysis B: Environmental

journal homepage: www.elsevier.com/locate/apcatb

Photoreduction of CO_2 on ZIF-8/TiO_2 nanocomposites in a gaseous photoreactor under pressure swing

Ehsan Pipelzadeh[a,b], Victor Rudolph[a], Graeme Hanson[c,1], Christopher Noble[c], Lianzhou Wang[a,b,*]

[a] School of Chemical Engineering, The University of Queensland, St Lucia QLD 4072, Australia
[b] Nanomaterials Centre, School of Chemical Engineering and Australian Institute for Bioengineering and Nanotechnology, The University of Queensland, St Lucia, QLD, 4072, Australia
[c] Center If Advance Imaging, The University of Queensland, QLD 4072 Australia

ARTICLE INFO

Article history:
Received 5 March 2017
Received in revised form 13 June 2017
Accepted 19 June 2017
Available online 20 June 2017

Keywords:
ZIF/TiO_2 composite
Photoreduction
CO_2 conversion
Pressure swing
Photoreactor

ABSTRACT

A new type of zeolitic imidazolate framework ZIF-8/TiO_2 nanocomposites was developed for photocatalytic reduction of CO_2 to CH_4 and CO in a newly designed photoreactor under intentionally controlled pressure swing. The ZIF-8/TiO_2 core-shell structure plays an important role in the adsorption of CO_2 by ZIF-8 and subsequent in-situ photocatalytic reduction on TiO_2. The introduction of pressure change in the reaction system facilitates the adsorption-desorption process of CO_2 and reaction products, which consequently led to improved photoreduction performance. This approach highlights the importance of mass transfer and reactor design for improved photoreduction.

1. Introduction

Fossil fuels are the main source of world's energy, but their use produces CO_2 at a rate far beyond sustainable environmental sinks. Reacting CO_2 back to chemical fuels, using photocatalytic reduction processes, is an attractive process initially introduced by Halmann et al. [1] Since then over 130 types of photocatalytically active materials have been developed and tested in various liquid and gaseous photo-reactors [2,3]. The photocatalytic process is a complex, multi-step surface redox reaction initiated by electron-hole separation and transfer derived from the semiconducting characteristics of the catalyst materials [4]. For CO_2 reduction on catalysts, CO_2 electron affinity is relatively high (−1.9 eV) which is lowered when it disorients from its stable liner structure into a less stable bent structure upon adsorption [5].

Despite decades of research effort, photoreduction processes are limited by a number of challenges, including low photoreduction yield and photocatalyst poisoning by products and intermediates [3,6]. Some of the strategies to address these issues are to tune the CO_2 surface interaction with photocatalyst to increase reactant loading, and to alter CO_2 molecule geometry via surface chemistry interactions for reactions to proceed and for products to be desorbed from reactive sites. From catalyst design and selection viewpoints, metal organic frameworks (MOF) have been considered as an excellent catalyst support system due to their high capacity to capture and reduce CO_2 [7]. Zeolitic imidazolate frameworks (ZIF) are a subclass of MOFs featuring excellent CO_2 uptake and simple fabrication. In conjugation with other photocatalytic materials it can improve the photocatalytic activity in aqueous and gaseous media [8,9]. For instance, ZIF-9 is shown to activate CO_2 leading to positive shift in the onset potential in photoelectrochemical CO_2 conversion process [10]. This is also evident using carbon aerogel as a substrate [11]. Thus we considered to design a new type of core-shell ZIF/TiO_2 nanocomposites which are expected not only to make good use of the CO_2 adsorption function of ZIF materials and but also to in-situ photocatalytically convert CO_2 on well-studied TiO_2 materials.

In addition to intensive research effort in searching new catalyst materials, very limited attention has been paid to the reactor configuration and process operations which are equally important for enhancing mass transfer and separation of products and intermediates from surface active sites. In terms of reactor design, slurry based photoelectrochemical reactors are generally favored in the

* Corresponding author.
E-mail address: l.wang@uq.edu.au (L. Wang).
[1] Deceased in late 2015.

http://dx.doi.org/10.1016/j.apcatb.2017.06.054
0926-3373/

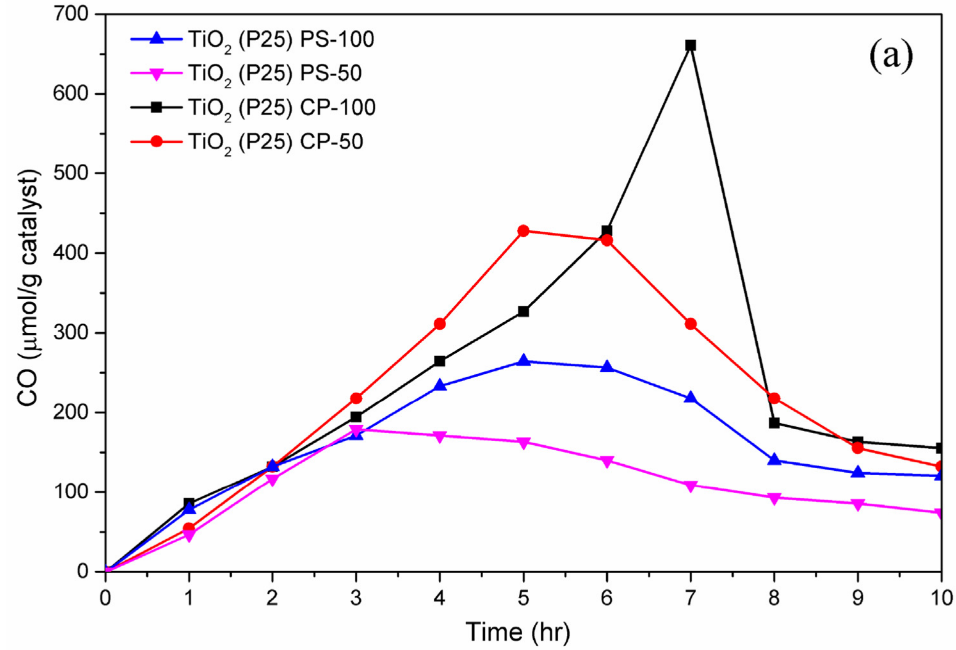

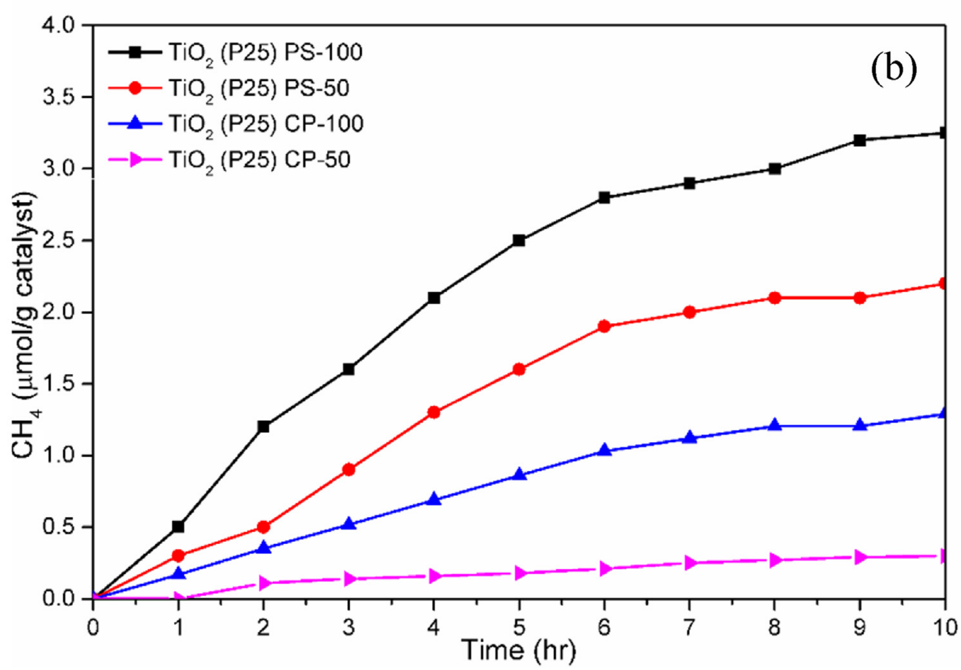

Fig. 1. (a) CO and (b) CH_4 yields as a function of illumination time on TiO_2 (P25) under various flow rates and pressure conditions.

literature due to their relative simplicity and ease of operation. The main drawback, however, is that the CO_2 loading in aqueous media is low even under alkaline condition or high CO_2 partial pressure [12,13]. In addition, aqueous system is disadvantaged because protons compete for electrons more readily than CO_2 to generate H_2 gas. Common arrangements in using gaseous reactors include fixed beds, optical fibers and honeycomb monoliths, using water and hydrogen as electron and hydrogen sources [14], while these still suffer from low CO_2 conversion efficiency. Herein we report a new approach achieving significant increase in photocatalytic CO_2 reduction to produce CO by rationally designing composite catalysts to increase reactant loading, and by introducing a new gaseous photoreactor with tuned reactor pressure to reduce mass transfer resistance and product desorption.

2. Experimental section

2.1. Catalyst preparation

2.1.1. ZIF-8 synthesis

ZIF-8 was prepared in aqueous media. 0.117 g of zinc nitrate $(Zn(NO_3)_2 . 6H_2O$ was dissolved in 80 ml of milli-Q water. 2.27 g of 2-methyl imidazole was also dissolved in 80 ml of milli-Q water. The solutions were mixed, spontaneously forming a milky white

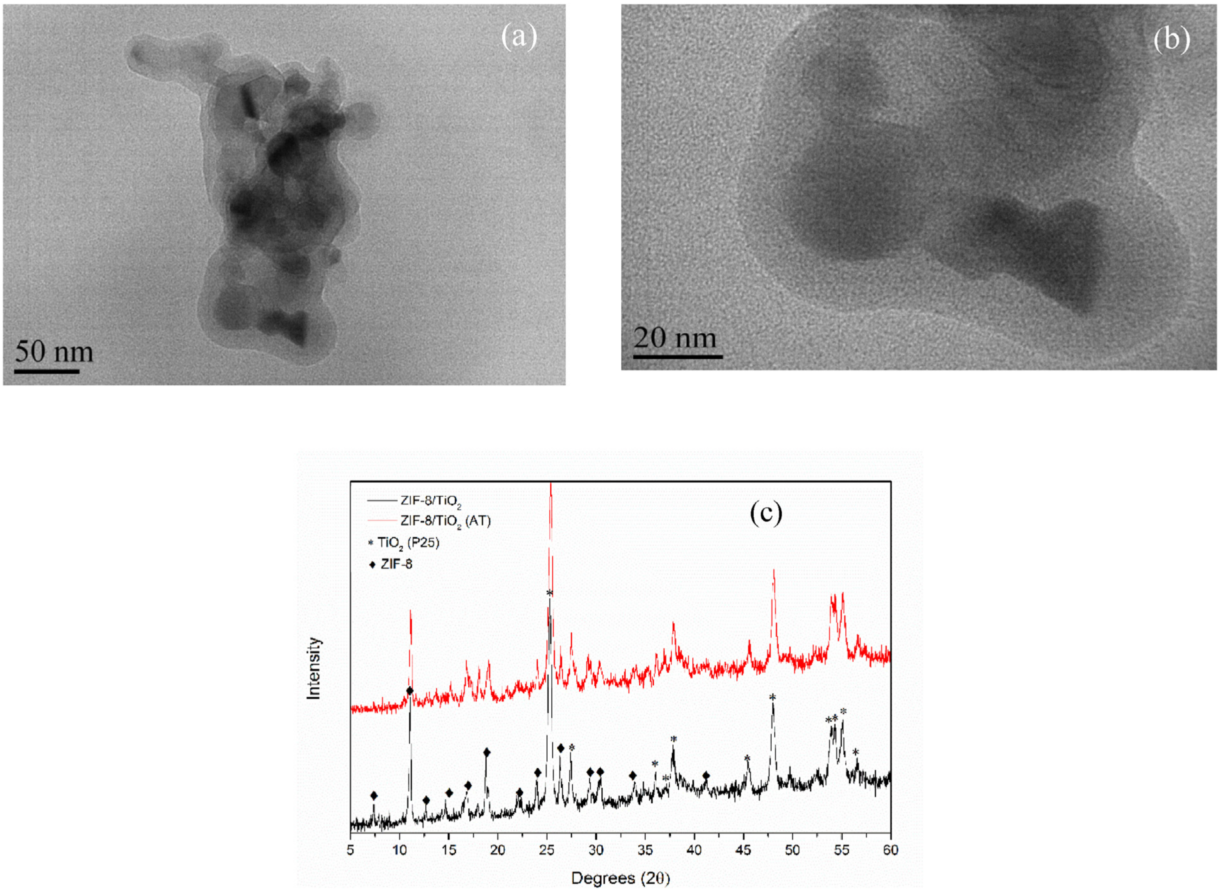

Fig. 2. (a) TEM and (b) HRTEM images of ZIF-8/TiO_2 core-shell structure, (c) XRD patterns of ZIF-8/TiO_2 nanocomposite before and after test (AT).

suspension. The mixture was stirred for 5 minutes followed by centrifuging at 15,000 rpm for 10 minutes. The resultant sample was washed using MilliQ water for a number of times and finally vacuum dried at 80 °C overnight to obtain the ZIF-8 samples.

2.1.2. ZIF-8/TiO_2 synthesis

Titanium dioxide (P25) was purchased and used as received. TiO_2/ZIF-8 core-shell nanocomposites were prepared in a sequential step-by-step process, consisting of the following steps; TiO_2 (P25) was dispersed in zinc nitrate (100 mmol) solution under ultrasonic treatment for 5 minutes. The suspension was centrifuged at 4500 rpm and washed with MilliQ water twice. Subsequently 2-methyl-immidazole (100 mmol) was added to the re-dispersed TiO_2 nanoparticle suspension to form ZIF-8 coating layer on the surface of TiO_2, and the suspension was also ultrasonically treated or 5 min. The bath temperature was controlled at 50 °C. The suspension was centrifuged at 4500 rpm and washed as before. This cycle was repeated for 10 consecutive times to obtain the ZIF-8/TiO_2 core-shell type nanocomposites.

2.2. ZIF-8/TiO_2 calcination

ZIF-8/TiO_2 composites were calcined under argon controlled atmosphere at rate 5 °C/min up to 300 °C and 400 °C respectively. The nanocomposite was kept at maximum temperature for 3 h before the temperature was dropped to room temperature.

2.3. Photocatalytic reactor

Closed-loop gaseous reactor comprising of a humidifier and a window reactor equipped with simulated sunlight was fabricated and used (Supporting Information, Fig. S1). A series of photocatalytic reduction tests were conducted and the results from the average of two consecutive repeatable tests used for presenting the results. The operation was under either constant pressure (CP) (5 bar) or pressure swing (PS) to mimic breathing (5–3 bar). The circulation gas flow with the rates of 50, 100 ml/min and pressure swing, were applied by a syringe type pump (Teledyne ISCO D260). Pressure rates change at 0.4 bar/min and 0.8 bar/min under pressure swing at 50 ml/min (PS-50) and 100 ml/min (PS-100) modes respectively. The catalysts were a new type of combined MOF and TiO_2 nanocomposites, ZIF-8/TiO_2 core-shell structure, prepared as described in experimental section. A series of background experiments were performed to evaluate the fabricated photocatalytic material using commercial TiO_2 (Degussa P25) and process for CO_2 photocatalytic reduction (supporting information).

2.4. Sample characterization

The X-ray diffraction (XRD) measurements were conducted on a Rigaku Miniflex XRD instrument with Co Kα (λ = 1.78897 Å) radiation. Plot is Cu corrected. Samples were prepared and tested in powder form. The transmission electron microscopy (TEM) images were taken using a high resolution TEM (HRTEM) using a JEOL JEM 2100. Samples were dispersed in aqueous media and collected using copper grids. Scanning electron microscopy (SEM) images were collected using JEOL 7100. Samples were dispersed in aqueous media and drop dried on SEM holder. The absorption spectra were measured using a Shimadzu 2200 UV–vis spectrometer. Spectra were collected in powder form. Thermal gravimetric analysis (TGA) was performed using alumina crucibles in a TGA/DSC STARe System, Mettler Toledo. The test was conducted in air and

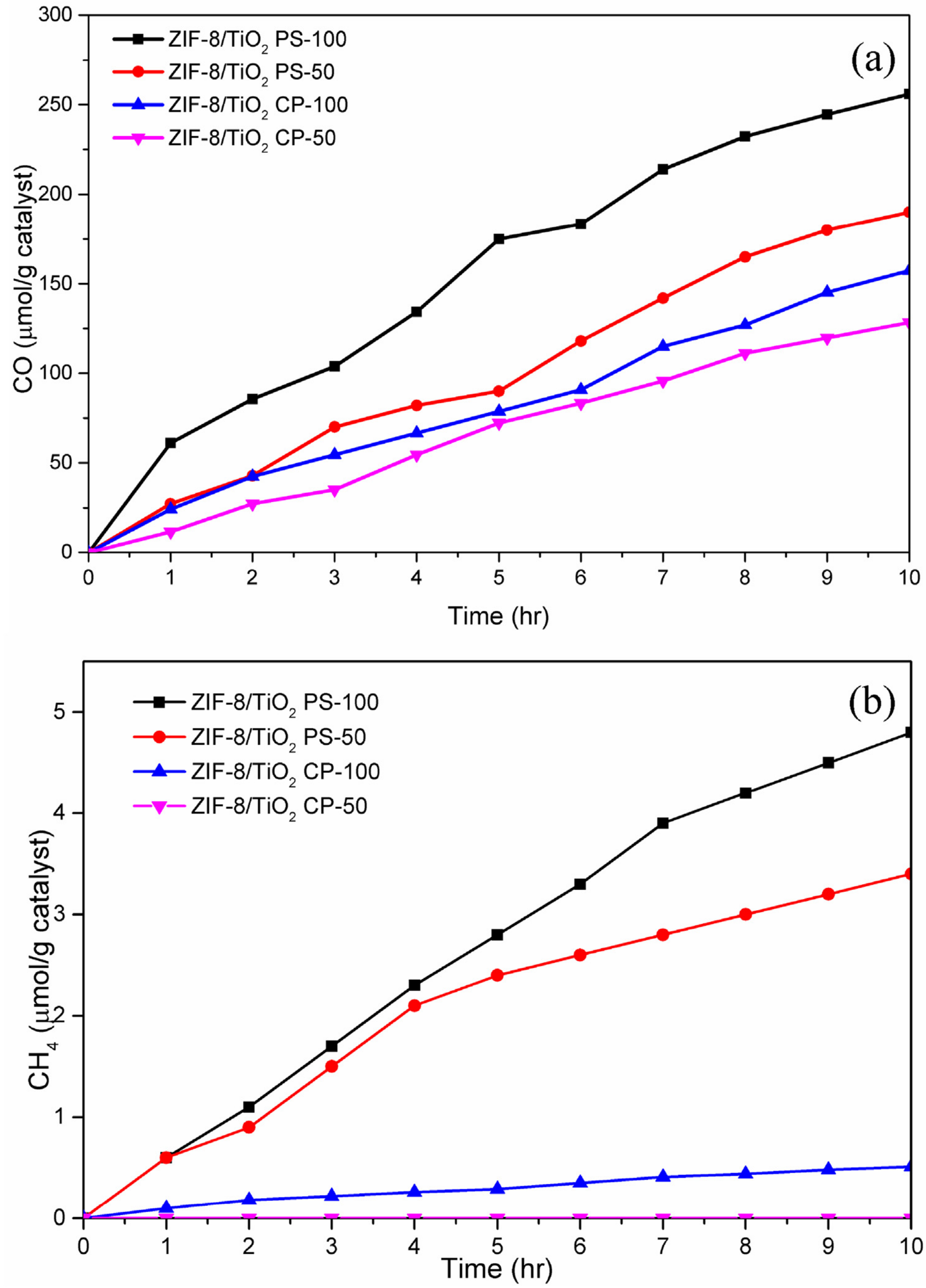

Fig. 3. (a) CO, and (b) CH_4 yields as a function of illumination time for ZIF-8/TiO_2 under various flow rates and pressure conditions.

argon controlled environment. The heating rate was set at 1 °C/min. Samples were dried and stored under room conditions. SERS spectra were collected on a Thermo-Fischer Almega dispersive Raman spectrometer. The instrument is fitted with 633 nm lasers, and spectra were collected at this excitation wavelength. The spectra were collected using a single grating, in high resolution mode, a slit width of 25 mm, an acquisition time of 1 s and an average of at least 128 spectra. Electro paramagnetic resonance spectroscopy (EPR) spectra were recorded using a Bruker ELEXSYS cw EPR spectrometer using a shq cavity and an ER4131VT liquid nitrogen cooling system. Samples were tested in dry form. Weight of the samples was measured for normalization purposes. Samples were degassed at 473 K and at pressure of 50 torr for 24 hr prior to CO_2 and N_2 sorption measurements. Specific surface areas (SBET) were calculated by the Brunauer-Emmett-Teller method at the relative pressures in the range of P/P0 = 0.05 – 0.30; and volumes of micropores were calculated from both the 77 K N_2 and 273 K CO_2 isotherms using the Dubinin-Astakhov (D-A) equation using Micromeritics Tristar 3020 system. The micropore surface area was calculated using Dubinin-Radushkevich (D-R) equation on the CO_2 adsorption data at 273 K. Angilent Technology 7820 GC System and HayeSep Q column was used for CO and CH_4 characterization. Gas tight syringe (100 ml) was used for sample injection. Calibration curves were prepared using calibrated gases and gas mixtures prepared using known glass volumes. Varian 3900 equipped with Resteck Rt®-Q-BOND was used to confirm the methane results.

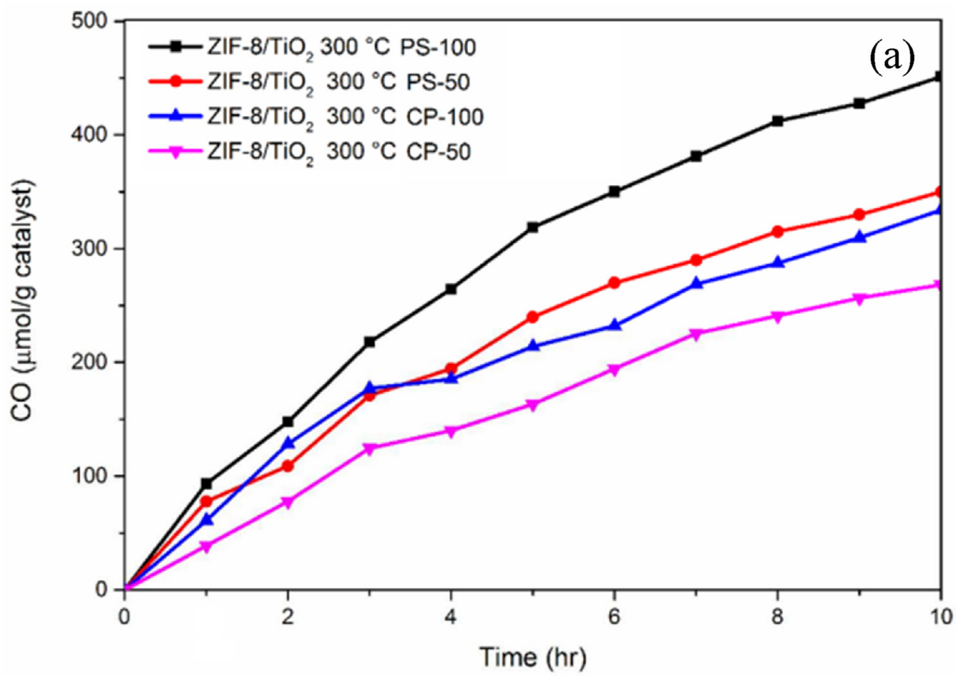

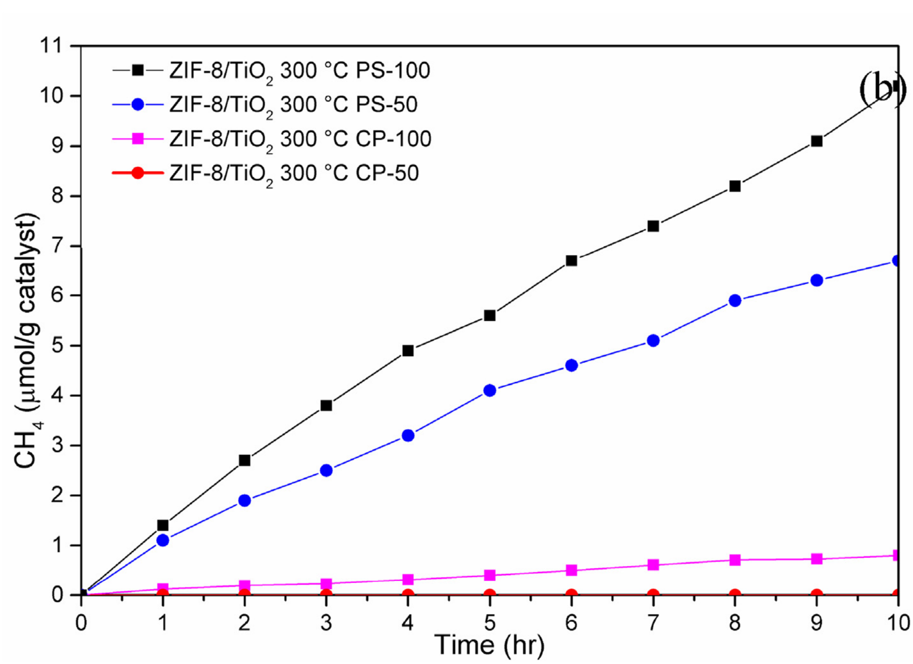

Fig. 4. (a) CO, and (b) CH_4 yields as a function of illumination time for ZIF/8TiO_2 calcined at 300 °C at various flow rates and pressure conditions.

3. Results and discussion

3.1. Photocatalytic CO_2 reduction

The reactor arrangement was tested first using P25 TiO_2, a widely recognized and well characterized photocatalyst. As indicated in Fig. 1, under CP of 5 bar the CH_4 and CO production rates are improved as the circulation rate is increased from 50 ml/min to 100 ml/min. In reaction engineering, this can be classically associated with a system that is limited by the mass transfer film resistance [15]. Increasing the level of turbulence near the catalyst surface reduces the mass transfer film resistance, with diminishing returns as other rate limitations (e.g. diffusion or reaction kinetics) become dominant. Note that due to the constraint of our current reactor arrangement, even at the highest pump circulation capacity of 100 ml/min, it is evident that mass transfer is still the limiting parameter, indicating that maximum conversion rates is not reached for this setup. In this regard, further optimization is required in our future work, yet the finding reported herein implies the importance of mass transfer in the photocatalytic reaction. These tests show the extent of CO_2 photoreduction with water as the source of electrons and protons in the presence of light yields more CO than CH_4 under all tested conditions. Other stoichiometry products such as hydrogen and oxygen were not detected which

may be due to detection limit of the GC used in the reaction system. Electrochemical reduction potentials indicate that CH_4 is thermodynamically more favored and is often observed as the final product in other studies, whereas CO (which requires only 2 electrons and protons compared with 8 electrons and protons for CH_4) is a kinetically favored intermediate [16]. It is likely the higher circulation gas flow rates increase bulk mass transfer, facilitating the release of CO from the catalyst surface before it can be further hydrogenated or oxidized, thus resulting in increased yield.

Very interestingly, the PS mode is found to remarkably increase the CO yield to 13.2 μmol/g h^{-1} (PS-50, 80% increase over CP-50 operation) and 15.6 μmol/g h^{-1} CO (PS-100, 30% increase over CP-100). It is also clear that the PS mode promotes CO production more than CH_4. This can be attributed to continuous alteration of the reactants and product adsorption/desorption on the photocatalyst surface, favoring regeneration of the Ti^{3+} active sites which are considered to be generally responsible for TiO_2 photocatalytic activity and will be discussed in following section [17]. Furthermore, an increase in gas flow rate facilitates CO removal and avoids quick catalyst poisoning. Previous studies have shown that CO and CO_2 compete for the same surface active sites [18], thus an increase in CO removal rate and dilution in the gas mixture is advantageous for catalyst life and product yield.

However, the yield and rate of CO generation dramatically reduces after several hours, as shown in Fig. 1. This change in catalyst activity of interest, and we speculate that CO oxidation to CO_2 and loss of active sites on photocatalyst might be attributable to the change. To better understand this change, we conduced electron paramagnetic resonance (EPR) spectroscopy analysis. As revealed by Fig. S2, a decrease in Ti^{3+} active sites in anatase and rutile phase at 1.981 and 1.970 g is evident, suggesting that some intermediate products were produced over time which could poison the active sites. This observation led us to deduce that for the purpose of photoreduction performance improvement, the protection of photocatalyst from deactivation is important and the back reaction (oxidation of CO) should be avoided. The TiO_2 (P25) was consequently modified by adding a thin layer of microporous zeolitic imidazolate framework (ZIF-8) to form a core-shell structure. The selection of ZIF-8 shell was based on the considerations of providing excellent CO_2 capture capacity and water tolerance [19], and protecting further oxidation of the synthesized products as it exhibited a high cut off ratio for CH_4 to CO_2 [20].

The ZIF-8/TiO_2 core-shell nanocomposite was fabricated using a step-by-step self-assembly method (more details in supporting information). The structure of ZIF-8/TiO_2 core-shell nanocomposite is shown in TEM images (Fig. 2(a) and (b)). The shell appears uniform and approximately 10 nm thick. The coated ZIF-8 is crystalline as confirmed by X-ray diffraction (XRD) pattern (Fig. 2c). To further examine the interface between the TiO_2 and ZIF-8 layers Raman spectroscopy was utilized (Fig. S3). The spectrum revealed the presence of Zn-O-Ti structure evident by peaks at 740, 1048 and 1128 cm^{-1} [21]. Addition peaks are also observed at 575 cm^{-1} which corresponds to E_1(LO) mode, indicating the presence of defects on the ZnO layer (Figs. 3 and 4).

The as-prepared nanocomposite was in cream colour. UV–vis absorption spectroscopy (Fig. S4) presents a distinctive red-shift to the visible region for core-shell structure compared to TiO_2 (P25). This suggests an interaction between two components might lead to visible light absorption. This is further confirmed by EPR spectroscopy (Fig. S5). It is shown that Ti^{3+} species was reduced upon ZIF-8 introduction. This highlights the involvement of surface active species in ZIF-8 framework. Furthermore; nanocomposite has extra signals along with Ti^{3+} signals in anatase and rutile, which were identified to be at $g_{x,y,z}$ 2.0023, 2.0063 and 2.01021, possibly corresponding to new radical centers which involve interaction between the ZIF-8 and TiO_2 surface. It is worth noting that these peaks were not distinguished when TiO_2 nanoparticles were replaced with SiO_2 nanoparticles, suggesting the signals are mainly associated with surface interactions between TiO_2 and ZIF-8. N_2 and CO_2 adsorption-desorption studies using CO_2 and N_2 (Figs. S6 and S7) show improvement in CO_2 uptake on ZIF-8/TiO_2 (P25) core-shell structure but N_2 uptake is reduced. This suggests the molecular sieve structure of ZIF-8 is important for reactant uptake.

Photocatalytic experiments on the core-shell structures indicate that the CO_2 photoreduction yield was steady for the composite catalyst over the full 10-hour reaction run. The catalyst performance was improved under PS mode and increase in gas flow rate. The CO production rate was 12.8 (CP-50) and 15.76 (CP-100) μmol/g h^{-1} respectively. This shows ~73% and 19% improvement compared to TiO_2 (P25) under same conditions, respectively. However; at CP mode CH_4 production was depressed to below detection limit for CP-50 condition and merely 0.052 μmol/g h^{-1} for CP-100 condition. This clearly highlights the impact of molecular sieve structure of ZIF-8, resulting in CH_4 trapping and subsequent oxidation. In PS mode CO yield increased to 19 and 25.6 μmol/g h^{-1} at 50 ml/min and 100 ml/min flow rate respectively. This corresponds to an improvement of 48% and 62% over the corresponding CP cases. CH_4 generation is improved under PS mode to 0.34 (PS-50) and 0.48 (PS-100) μmol/g h^{-1} respectively. This indicates the presence of ZIF-8 facilitates CH_4 generation and the pressure gradient has determinative role in product removal. An examination of the nanocomposite catalyst after reaction revealed a color change from cream yellow to dark yellow (Fig. S8). This suggests that the material was undergoing some change during the reaction. XRD patterns revealed the peak intensities for ZIF-8 were lowered after test (AT) (Fig. 2C), indicating the structure of the nanocomposite is unstable. Physical mixing of TiO_2 and ZIF-8 was performed and the resultant mixture was tested, but no improvement in the CO_2 reduction was not found.

The ZIF-8/TiO_2 was consequently calcined in an argon atmosphere at temperatures of 300 °C and 400 °C. The effect of calcination was analyzed using TGA-DSC (Figs. S10 and S11). Calcined catalyst was light brown to dark brown (an increase in visible region absorption (Fig. S12)) at 300 °C and 400 °C respectively. This suggests carbonization of the ZIF-8 layer, which is evident by carbon centered radicals indicate by g value of approximately 2.0034 by EPR spectroscopy (Fig. S13). Additionally; EPR analysis did not show any noticeable Ti^{3+} sites which are commonly considered as active sites for CO_2 adsorption and reduction. Further morphological studies show the catalyst structure is aggregated forming sheet-like structures at higher temperatures (Fig. S14). ZIF-8 structure is partially changed upon calcination which is evident by increase in N_2 uptake and reduction in CO_2 uptake (Figs. S5 and S6). Encouragingly, the calcined catalyst at 300 °C was crystalline and stable during photoreduction test, implying the better structural stability upon calcination (Fig. S15).

Photoreduction results indicates that CO yield is stable and most efficient at higher pressure fluctuation rates, for instance, 45.16 μmol/g h^{-1} under PS-100 condition. Whereas under CP mode, CO yield is 33.4 6 μmol/g h^{-1} at the same flow rate. This is in good agreement to the trend observed above, suggesting product removal step is one of the most determining steps in photoreduction productivity. Note that the product generation is progressive without clear indication of catalyst poisoning. While calcined catalysts show similar CO_2 uptake, sample calcined at 300 °C was evident to be more desirable for CO and CH_4 yield as photoreduction performance was reduced for samples calcined at 400 °C (Fig. S16).

4. Conclusions

In summary, we reported the CO_2 photoreduction under intentionally controlled pressure swing which affects product yield and catalyst lifetime. High CO yield was achieved by introducing a ZIF-8 layer on TiO_2 based photocatalyst, which facilitated CO_2 loading on catalyst and its subsequent in-situ photoreduction. Further controlled calcination of ZIF-8/TiO_2 composite was found beneficial towards higher CO yield and stable catalysts. The findings reported here may provide better understanding on the photocatalytic CO_2 reaction system, in particular the importance of reactor design and conditions for efficiency improvement.

Acknowledgement

Financial support from Australian Research Council through its Discovery and Future Fellowship schemes is appropriated.

Appendix A. Supplementary data

Supplementary data associated with this article can be found, in the online version, at http://dx.doi.org/10.1016/j.apcatb.2017.06.054.

References

[1] M. Halmann, Photoelectrochemical reduction of aqueous carbon dioxide on p-type gallium phosphide in liquid junction solar cells, Nature 275 (5676) (1978) 115–116.
[2] S. Das, W.M.A. Wan Daud, Photocatalytic CO_2 transformation into fuel: a review on advances in photocatalyst and photoreactor, Renew. Sustain. Energy Rev. 39 (2014) 765–805.
[3] S.N. Habisreutinger, L. Schmidt-Mende, J.K. Stolarczyk, Photocatalytic reduction of CO_2 on TiO_2 and other semiconductors, Angew. Chem. Int. Ed. 52 (29) (2013) 7372–7408.
[4] Q. Kang, et al., Photocatalytic reduction of carbon dioxide by hydrous hydrazine over Au–Cu Alloy nanoparticles supported on $SrTiO_3/TiO_2$ coaxial nanotube, Angew. Chem. 3 (2015) 855–859.
[5] A. Markovits, A. Fahmi, C. Minot, A theoretical study of CO_2 adsorption on TiO_2, J. Mol. Struct.: Theochem. 371 (1996) 219–235.
[6] S. Navalón, et al., Photocatalytic CO_2 reduction using non-titanium metal oxides and sulfides, ChemSusChem 6 (4) (2013) 562–577.
[7] W.-N. Wang, et al., Comparison of CO_2 photoreduction systems: a review, Aerosol Air Qual. Res. 14 (2) (2014) 533–549.
[8] C.-H. Kuo, et al., Yolk–shell nanocrystal@ ZIF-8 nanostructures for gas-phase heterogeneous catalysis with selectivity control, J. Am. Chem. Soc. 134 (35) (2012) 14345–14348.
[9] Q. Liu, et al., ZIF-8/Zn_2GeO_4 nanorods with an enhanced CO_2 adsorption property in an aqueous medium for photocatalytic synthesis of liquid fuel, J. Mater. Chem. A 1 (38) (2013) 11563–11569.
[10] Q. Shen, et al., Biomimetic photoelectrocatalytic conversion of greenhouse gas carbon dioxide: two-electron reduction for efficient formate production, Appl. Catal. B: Environ. 201 (2017) 70–76.
[11] X. Huang, et al., A CO_2 adsorption-enhanced semiconductor/metal-complex hybrid photoelectrocatalytic interface for efficient formate production, Energy Environ. Sci. 9 (10) (2016) 3161–3171.
[12] A.D. Handoko, J. Tang, Controllable proton and CO_2 photoreduction over Cu_2O with various morphologies, Int. J. Hydrogen Energy 38 (29) (2013) 13017–13022.
[13] M. Gattrell, N. Gupta, A. Co, A review of the aqueous electrochemical reduction of CO_2 to hydrocarbons at copper, J. Electroanalyt. Chem. 594 (1) (2006) 1–19.
[14] K. Li, et al., A critical review of CO_2 photoconversion: catalysts and reactors, Catal. Today 224 (0) (2014) 3–12.
[15] H. Fogler, External diffusion effects on heterogeneous reactions, Elements Chem. React. Eng. 2006 (2016) 757–801.
[16] I.A. Shkrob, et al., Photoredox reactions and the catalytic cycle for carbon dioxide fixation and methanogenesis on metal oxides, J. Phys. Chem. C 116 (17) (2012) 9450–9460.
[17] M. Anpo, et al., Photocatalytic reduction of CO_2 with H_2O on various titanium oxide catalysts, J. Electroanalyt. Chem. 396 (1–2) (1995) 21–26.
[18] A. Fahmi, C. Minot, A theoretical study of CO adsorption on TiO_2, J. Organomet. Chem. 478 (1–2) (1994) 67–73.
[19] D. Ge, H.K. Lee, Water stability of zeolite imidazolate framework 8 and application to porous membrane-protected micro-solid-phase extraction of polycyclic aromatic hydrocarbons from environmental water samples, J. Chromatogr. A 1218 (47) (2011) 8490–8495.
[20] G. Lu, et al., Imparting functionality to a metal–organic framework material by controlled nanoparticle encapsulation, Nat. Chem. 4 (2012) 310–316.
[21] B.S. Shaheen, et al., Thermal/electrochemical growth and characterization of one-dimensional ZnO/TiO_2 hybrid nanoelectrodes for solar fuel production, J. Phys. Chem. C 117 (36) (2013) 18502–18509.